

RESEARCH

Open Access



The putative proton-coupled organic cation antiporter is involved in uptake of triptans into human brain capillary endothelial cells

Nana Svane¹, Alberte Bay Villekjær Pedersen¹, Anne Rodenberg¹, Burak Ozgür^{1,2}, Lasse Saaby^{1,3}, Christoffer Bundgaard⁴, Mie Kristensen¹, Peer Tfelt-Hansen⁵ and Birger Brodin^{1*}

Abstract

Background Triptans are anti-migraine drugs with a potential central site of action. However, it is not known to what extent triptans cross the blood–brain barrier (BBB). The aim of this study was therefore to determine if triptans pass the brain capillary endothelium and investigate the possible underlying mechanisms with focus on the involvement of the putative proton-coupled organic cation (H⁺/OC) antiporter. Additionally, we evaluated whether triptans interacted with the efflux transporter, P-glycoprotein (P-gp).

Methods We investigated the cellular uptake characteristics of the prototypical H⁺/OC antiporter substrates, pyrilamine and oxycodone, and seven different triptans in the human brain microvascular endothelial cell line, hCMEC/D3. Triptan interactions with P-gp were studied using the IPEC-J2 MDR1 cell line. Lastly, *in vivo* neuropharmacokinetic assessment of the unbound brain-to-plasma disposition of eletriptan was conducted in wild type and *mdr1a/1b* knockout mice.

Results We demonstrated that most triptans were able to inhibit uptake of the H⁺/OC antiporter substrate, pyrilamine, with eletriptan emerging as the strongest inhibitor. Eletriptan, almotriptan, and sumatriptan exhibited a pH-dependent uptake into hCMEC/D3 cells. Eletriptan demonstrated saturable uptake kinetics with an apparent K_m of $89 \pm 38 \mu\text{M}$ and a J_{max} of $2.2 \pm 0.7 \text{ nmol}\cdot\text{min}^{-1}\cdot\text{mg protein}^{-1}$ ($n = 3$). Bidirectional transport experiments across IPEC-J2 MDR1 monolayers showed that eletriptan is transported by P-gp, thus indicating that eletriptan is both a substrate of the H⁺/OC antiporter and P-gp. This was further confirmed *in vivo*, where the unbound brain-to-unbound plasma concentration ratio ($K_{p,uu}$) was 0.04 in wild type mice while the ratio rose to 1.32 in *mdr1a/1b* knockout mice.

Conclusions We have demonstrated that the triptan family of compounds possesses affinity for the H⁺/OC antiporter proposing that the putative H⁺/OC antiporter plays a role in the BBB transport of triptans, particularly eletriptan. Our *in vivo* studies indicate that eletriptan is subjected to simultaneous brain uptake and efflux, possibly facilitated by the putative H⁺/OC antiporter and P-gp, respectively. Our findings offer novel insights into the potential central site of action involved in migraine treatment with triptans and highlight the significance of potential transporter related drug–drug interactions.

Keywords Blood–brain barrier, Capillary endothelium, Triptans, Migraine treatment, Proton-coupled organic cation antiporter, P-glycoprotein, Oxycodone transporter, Active uptake

*Correspondence:

Birger Brodin

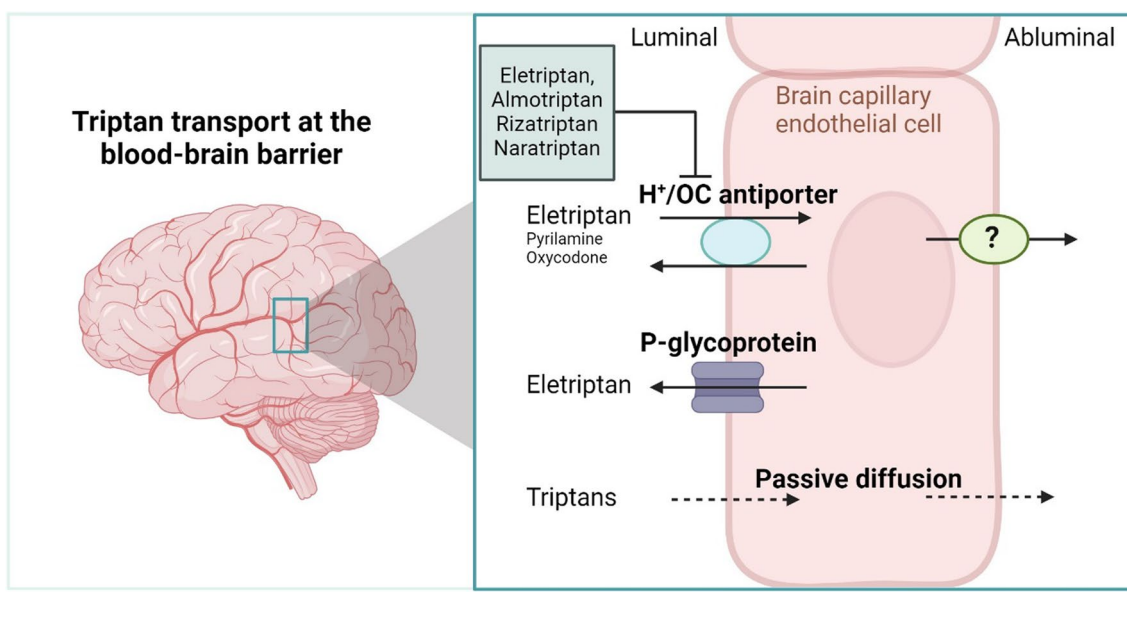
birger.brodin@sund.ku.dk

Full list of author information is available at the end of the article



© The Author(s) 2024. **Open Access** This article is licensed under a Creative Commons Attribution 4.0 International License, which permits use, sharing, adaptation, distribution and reproduction in any medium or format, as long as you give appropriate credit to the original author(s) and the source, provide a link to the Creative Commons licence, and indicate if changes were made. The images or other third party material in this article are included in the article's Creative Commons licence, unless indicated otherwise in a credit line to the material. If material is not included in the article's Creative Commons licence and your intended use is not permitted by statutory regulation or exceeds the permitted use, you will need to obtain permission directly from the copyright holder. To view a copy of this licence, visit <http://creativecommons.org/licenses/by/4.0/>. The Creative Commons Public Domain Dedication waiver (<http://creativecommons.org/publicdomain/zero/1.0/>) applies to the data made available in this article, unless otherwise stated in a credit line to the data.

Graphical Abstract



Background

Migraine is a common chronic neurological disorder affecting more than 10% of the population [1, 2]. Triptans are a class of tryptamine-based compounds used in the treatment of migraine. The seven triptans in clinical use are sumatriptan, almotriptan, eletriptan, frovatriptan, naratriptan, rizatriptan, and zolmitriptan [3]. Triptans are potent agonists of the $5HT_{1B/1D}$ receptors that are found on smooth muscle cells in the intracranial extracerebral vasculature, where activation results in the constriction of the vasculature and hereby relief of migraine symptoms [4, 5]. Furthermore, triptans inhibit the release of vasodilating and inflammatory substances from the trigeminal nerve [4, 5]. In addition to these peripheral effects, several factors indicate that triptans may act on $5HT_{1B/1D}$ receptors within the central nervous system (CNS), but the mechanism by which this occurs is poorly understood [6, 7].

Triptans are relatively hydrophilic compounds carrying a positive charge at physiologically relevant pH. As a consequence, triptans are expected to exhibit a limited ability to cross the restrictive blood–brain barrier (BBB) by passive diffusion [7]. However, common central side effects of triptans such as dizziness, fatigue, somnolence, and confusion, suggest that triptans enter the brain parenchyma to some extent [8, 9]. In addition, several preclinical studies have demonstrated a general disposition of triptans in the brain, as well as central $5HT_{1B/1D}$ receptor activation after systemic administration [10–16]. Both of

these observations indicate that triptans cross the BBB, possibly facilitated by carrier-mediated transport when considering the hydrophilic nature of this class of drug compounds.

A putative proton-coupled organic cation (H^+/OC) antiporter was discovered in the 1980's based on its function [17, 18]. More recent studies have provided functional and molecular identification of the H^+/OC antiporter, which differentiate from other known transporters [19–22]. The H^+/OC antiporter is suggested to transport substrates such as histamine receptor antagonists (pyrilamine and diphenhydramine) [19, 21, 23, 24], opioid agonists (oxycodone and tramadol) [19, 25], memantine (an NMDA receptor antagonist) [26], pramipexol (a dopamine 2 receptor agonist) [27], and nicotinic acetylcholine receptor agonists (nicotine and varenicline) [28, 29]. A number of these substrates are found to not only cross the BBB, but also to accumulate in the brain, as indicated by an unbound brain-to-unbound plasma partitioning coefficient ($K_{p,uu}$) above 1 [29–32]. A common trait among these H^+/OC antiporter substrates, is that they are small molecules bearing a secondary or tertiary amine moiety, which is positively charged at physiological pH [33, 34].

All triptans possess a secondary or tertiary amine moiety, which is positively charged at physiological pH, a common trait of H^+/OC antiporter substrates. We therefore hypothesized that triptans could be substrates of the H^+/OC antiporter, which could have significant

implications for their ability to cross the BBB. The aim of the present study was to investigate the potential involvement of the H⁺/OC antiporter in the uptake of triptans into brain capillary endothelial cells. Uptake and transport of triptans was investigated in the human brain microvascular endothelial cell line hCMEC/D3, which previously have been shown to functionally express the H⁺/OC antiporter [21, 25, 26, 29, 35, 36], in the IPEC-J2 MDR1 cell line over-expressing the human version of P-gp, and lastly in wild type and *mdr1a/1b* (P-gp) knock-out mice.

The rationale behind this study was to provide insights into the molecular mechanisms of triptan transport across the BBB with the long-term perspective of contributing to the central site of action hypothesis. This information can be helpful in the design of future antimigraine compounds to be either more or less BBB penetrable. In addition, the results of this study could reveal potential transporter-related drug-drug interactions in migraine therapy. We demonstrate that the majority of the tested triptans inhibited H⁺/OC antiporter-mediated uptake of pyrilamine, with eletriptan emerging as the strongest inhibitor. Eletriptan, almotriptan, and sumatriptan translocated into hCMEC/D3 cells in a pH-dependent manner, but only eletriptan demonstrated saturable uptake kinetics in the tested concentration range. Eletriptan was moreover confirmed to be a substrate of P-gp. Neuropharmacokinetic assessment of eletriptan demonstrated low brain uptake in wild type mice, but with dominating brain uptake in *mdr1a/1b* knockouts. Overall, we propose that the putative H⁺/OC antiporter is an uptake pathway for eletriptan at the brain endothelium, and that other triptans also interact with the transporter.

Methods

Materials

All chemicals were purchased from Merck (Soeborg, Denmark) unless otherwise stated.

Cell culture

The immortalized human cerebral microvascular endothelial cell line (hCMEC/D3) was maintained in T75-flasks coated with collagen type I from calf skin (C9791, 18.7 µg/mL) and cultured in EBM[®]-2 medium (Lonza, Basel, Schweiz) supplemented with 5% (v/v) fetal bovine serum (FBS, 10270, Life Technologies, CA, USA or SH3008803, ThermoFisher Scientific, MA, USA), 100 U/mL penicillin and 100 µg/mL streptomycin, 1 ng/mL human basic fibroblast growth factor (bFGF), 1.4 µM hydrocortisone, 1% (v/v) chemically defined lipid concentrate (ThermoFisher Scientific, MA, USA), 10 mM N-2-hydroxyethylpiperazine-N-2-ethane

sulfonic acid (HEPES) and 5 µg/mL ascorbic acid (5% CO₂, 37 °C). Culture media was changed every second or third day. Cells were passaged using trypsin–EDTA solution 10x (T4174, <5 min, 5% CO₂, 37 °C). For experiments, cells were seeded into 24-well plates (6.7·10⁴ cells/cm²) and cultured for four continuous days. The cells were used for experiments between passage 3–31.

The porcine ileum epithelial cell line IPEC-J2 transfected with human MDR1 [37] was maintained in T175-flasks and cultured in Dulbecco's Modified Eagle Medium/Nutrient Mixture F-12, supplemented with 10% (v/v) FBS (SH3008803, ThermoFisher Scientific, MA, USA), 100 U/mL penicillin and 100 µg/mL streptomycin, 2 mM L-glutamine, and 1 mM sodium pyruvate. The culture medium was supplemented with 2 µg/mL puromycin during maintenance. Culture media was changed every second or third day. Cells were passaged using trypsin–EDTA solution 10x (5–10 min, 5% CO₂, 37 °C). For experiments, cells were either seeded into 24-well plates (1·10⁵ cells/cm²) and cultured for 2 days or seeded on Transwell[®] polyester inserts (3460, 1.12 cm², pore size 0.4 µm) (3.57·10⁴ cells/cm²) and cultured for 15–17 days. IPEC-J2 MDR1 cells were used for experiments between passage 2–4.

Cellular uptake studies

The cells were washed twice with 37 °C Hank's Balanced Salt Solution (HBSS) supplemented with 10 mM HEPES, 0.0375% (v/v) sodium bicarbonate and 0.05% (w/v) bovine serum albumin (BSA) and adjusted to pH 7.4 (hHBSS). The cells were equilibrated in hHBSS with or without inhibitor for 15 min (37 °C, 90 rpm). The compound of interest was spiked into the hHBSS followed by incubation for a designated time. The timeframe of the initial uptake rate was validated into hCMEC/D3 cells (Fig. 1 and Additional file 1). The experiment was terminated by washing three times with ice-cold HBSS supplemented with 0.0375% (v/v) sodium bicarbonate.

To assess the concentration-dependent uptake, the uptake flux was fitted to the Michaelis–Menten equation, Eq. 1.

$$J_{ss} = \frac{J_{max}[S]}{K_m + [S]} \quad (1)$$

where J_{ss} represents flux under steady state, J_{max} is the maximal flux, $[S]$ is the substrate concentration, and K_m is the Michaelis–Menten constant.

The inhibitory constant at 50% inhibition (IC_{50}) was determined by fitting the uptake flux (J_{ss}) as function of the logarithmic inhibitor concentration to Eq. 2.

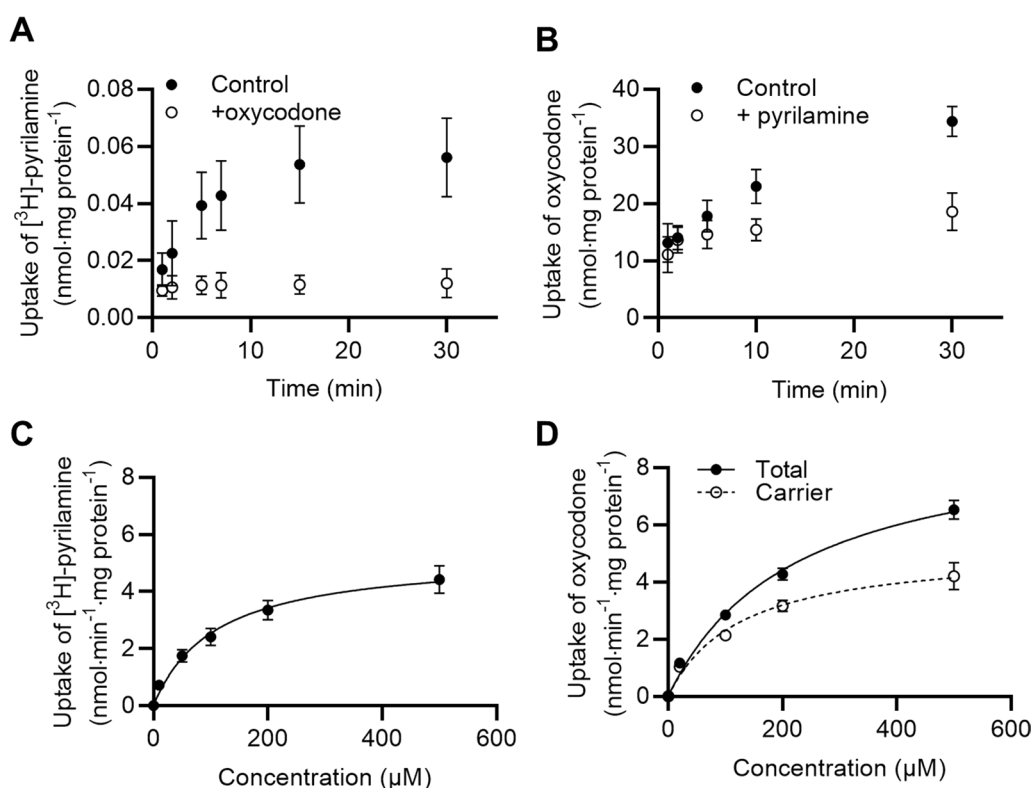


Fig. 1 Uptake kinetics of prototypical H^+ /OC antiporter substrates into hCMEC/D3 cells. **A** Time-dependent uptake of $[^3H]$ -pyrilamine (1 μ Ci/mL, 48 nM) in the absence (Control) or presence of 500 μ M oxycodone (+ oxycodone) ($n=2-3$, $N_{total}=6-9$). **B** Time-dependent uptake of oxycodone (500 μ M) in the absence (Control) or presence of 1000 μ M pyrilamine (+ pyrilamine) ($n=3$, $N_{total}=9$). **C** Concentration-dependent uptake of $[^3H]$ -pyrilamine (1 μ Ci/mL, 48 nM) in the presence of increasing concentrations of non-labelled pyrilamine. Data are fitted to non-linear regression (Michaelis–Menten kinetics) ($n=3$, $N_{total}=9$). **D** Concentration-dependent uptake of oxycodone in the presence of 1000 μ M pyrilamine. The total uptake is shown in closed circles, and the calculated carrier-mediated uptake (total—passive) is shown in open circles. Carrier-mediated uptake is fitted to non-linear regression (Michaelis–Menten kinetics) ($n=3$, $N_{total}=9$). All data points represent *mean* \pm *SD*. Uptake amounts are normalized against protein content per well

$$J_{ss} = J_{min} + \frac{(J_{max} - J_{min})}{1 + 10^{(\log(IC_{50}) - [I])n_H}} \quad (2)$$

where $[I]$ is the inhibitor concentration, n_H is the Hill coefficient.

The hCMEC/D3 cells were used for $[^3H]$ -pyrilamine inhibition studies between passage 3–6 (pyrilamine, oxycodone), 16–18 (almotriptan), 7–13 (eletriptan), 25–27 (frovatriptan), 3–8 (naratriptan), 16–18 (rizatriptan), 12–14 (sumatriptan), and 14–16 (zolmitriptan).

The hCMEC/D3 cells were used for time-dependent uptake studies between passage 3–5 (pyrilamine), 7–9 (oxycodone), 6–8 (almotriptan), and 24–31 (eletriptan).

The hCMEC/D3 cells were used for concentration-dependent uptake studies between passage 21–23 (pyrilamine), 11–13 (oxycodone), 12–14 (almotriptan), 16–18 (eletriptan), and 12–14 (sumatriptan).

The hCMEC/D3 cells were used for uptake studies of almotriptan, eletriptan, and sumatriptan in the presence of pyrilamine and oxycodone between passage 21–23.

The IPEC-J2-MDR1 cells were used for $[^3H]$ -digoxin inhibition studies between passage 2–4.

Manipulation of intra- and extracellular pH

Intracellular pH was manipulated as earlier described by Byron et al. [38] to assess the involvement of a proton antiporter, i.e. the H^+ /OC antiporter. Briefly, elevated intracellular pH during cellular uptake was achieved by adding the substrate of interests immediately (<10 s) after exposure to 30 mM NH_4Cl in hHBSS. Decreased intracellular pH during cellular uptake was achieved by preincubation with 30 mM NH_4Cl in hHBSS (30 min, 37 $^{\circ}C$) followed by aspiration and addition of hHBSS buffer. After approximately 60 s, the compound of interest was added to the buffer. Extracellular pH manipulation was achieved by adding hHBSS adjusted to pH 6.8, 7.4, or 8.2 during cellular uptake. The hCMEC/D3 cells were used for pH manipulation experiments between passage 17–19 (pyrilamine), 10–12 (oxycodone, almotriptan), 12–14 (eletriptan), and 3–5 (sumatriptan).

Intracellular pH measurements

Intracellular pH changes were assessed with the fluorescent pH indicator 2',7'-bis-(Carboxyethyl)-5(6')-carboxyfluorescein acetoxymethyl ester (BCECF-AM) using a NOVostar plate reader (BMG TABTECH GmbH, Offenburg, Germany). Fluorescence intensities were measured using a dual excitation of 485 and 380 nm and an emission filter of 520 nm. Briefly, hCMEC/D3 cells were seeded into a 96-well plate ($3 \cdot 10^4$ cells/cm²) and cultured for three continuous days (5% CO₂, 37 °C). Cell media was changed the day before an experiment. A 5 μM BCECF-AM loading solution was prepared in hHBSS without BSA (hHBSS(-)) followed by sonication using a tip sonicator S-4000 (60 amplitude, 120 s, Misonix, NY, USA), to boost dissolution, and equilibrated to 37 °C. The cells were washed twice with 37 °C hHBSS(-) and loaded with the BCECF-AM solution (45 min, protected from light, 37 °C). The cells were washed three times with 37 °C hHBSS(-) and loaded with either hHBSS(-) or 30 mM NH₄Cl in hHBSS(-). Control cells were preincubated with hHBSS(-) followed by automated injection of hHBSS(-) to validate the influence of injection on the fluorescence signal. Cells exposed to acute NH₄Cl were preincubated with hHBSS(-) followed by automated injection of NH₄Cl to a final concentration of 30 mM. For automated injections during measurements, the injection volume was 33 μL with a speed of 310 μL/s. Cells exposed to NH₄Cl preincubation were preincubated with 30 mM NH₄Cl in hHBSS(-) for 30–60 min followed by measurements of the fluorescent baseline. The NH₄Cl solution was manually aspirated followed by manual loading of 100 μL hHBSS(-). Immediately thereafter, the fluorescence was assessed. The fluorescent signal was normalized against baseline signals. The hCMEC/D3 cells were used for intracellular pH measurements between passage 26–28.

Barrier integrity measurements

The barrier integrity of the IPEC-J2 MDR1 cell monolayers cultured on semipermeable supports was assessed by transepithelial electrical resistance (TEER) measurements. Cells were allowed to equilibrate at room temperature for 20 min. The resistance was measured using an Endohm 12-cup electrode chamber (World Precision Instruments Inc., FL, USA) connected to an EVOM voltmeter (World Precision Instruments Inc., FL, USA). Measured TEER values were subtracted by the TEER value of a blank filter (14 Ω), normalized to the surface area of the permeable support (1.12 cm²), and expressed as Ω·cm². The IPEC-J2 MDR1 cells were used for barrier integrity measurements between passage 2–4.

Bidirectional transport

Bidirectional transport studies were conducted using IPEC-J2 MDR1 cell monolayers cultured on semipermeable Transwell® polyester inserts (Corning Inc., NY, USA, 3460, 1.12 cm², pore size 0.4 μm). The cells were washed twice with 37 °C hHBSS. Before initiation of the experiment, the cells were equilibrated in 37 °C hHBSS with or without zosuquidar (ZSQ) (2 μM) for 15 min (37 °C, 90 rpm). After equilibration, eletriptan HBr (50 μM) was spiked into the donor compartment. Samples were taken from the receiver compartment after 15, 30, 45, 60, 90, and 120 min. Samples of 100 μL were withdrawn from the basolateral compartment, while samples of 50 μL were withdrawn from the apical compartment. The withdrawn sample volume was immediately replaced with an equal volume of 37 °C hHBSS with or without ZSQ. Donor samples were sampled at the end of the experiment. The IPEC-J2 MDR1 cells were used in bidirectional transport experiments between passage 2–4.

The accumulated amount of drug (Q) was calculated for each time-point using Eq. 3.

$$Q = V_s \left(\sum_{n=1}^n C_{n-1} \right) + C_n V_t \quad (3)$$

where V_s represents the sample volume, V_t the total volume of the receiver compartment, C_n is the concentration of the sample n .

Steady state flux ($J_{\text{steady state}}$) was calculated as the slope of the linear part of the accumulated amount (Q) in the receiver compartment as function of time from Eq. 4.

$$J_{ss} = \frac{\Delta Q}{\Delta t \cdot A} \quad (4)$$

where t represents time and A is the area of the permeable support.

The apparent permeability (P_{app}) was calculated from Eq. 5.

$$P_{\text{app}} = \frac{J_{ss}}{C_{\text{donor}}} \quad (5)$$

where C_{donor} represents the initial concentration in the donor compartment.

Efflux ratios (ER) were calculated as the ratio of the apparent permeability in the basolateral to apical direction $P_{\text{app}}(\text{B-A})$ and the permeability in the apical to basolateral direction $P_{\text{app}}(\text{A-B})$ using Eq. 6.

$$\text{ER} = \frac{P_{\text{app}}(\text{B-A})}{P_{\text{app}}(\text{A-B})} \quad (6)$$

Sample preparation and quantification of radiolabeled compounds from in vitro experiments

The cells were permeabilized using 0.1% (v/v) Triton X-100 in ultrapure water (ELGA, Buckinghamshire, England) for 10 min at room temperature. Thereafter, the cells were scraped off the bottom of the wells, transferred to scintillation vials, and mixed with 2 mL of Ultima Gold 241 TM (Perkin Elmer, MA, USA). The samples were analyzed using a Tri-Carb 2910 TR Liquid Scintillation Analyzer (Perkin Elmer, MA, USA).

Sample preparation and quantification of unlabeled compounds from in vitro experiments

The cells were permeabilized using 50% (v/v) acetonitrile (HPLC LC-MS grade, VWR International S.A.S, Soeborg, Denmark) in ultrapure water (ELGA, Buckinghamshire, England) for 10 min at room temperature. Thereafter, the cells were scraped off the bottom of the wells and transferred to HPLC vials. Samples from bidirectional transport experiments were transferred directly into HPLC vials. All samples were stored at -18°C for later analysis. Calibration curves with standards in the range of 1 or 5–1000 ng/mL were dissolved in 50% (v/v) acetonitrile in ultrapure water (ELGA, Buckinghamshire, England), or in hHBSS(-) for analysis of bidirectional transport samples.

Liquid chromatography tandem mass spectrometry (LC-MS/MS) were performed using electrospray ionization in positive mode on a micromass Quattro microTM API tandem quadrupole mass spectrometer (Waters, MA, USA) or an Ultivo triple quadrupole mass spectrometer (Agilent Technologies, CA, USA) coupled to Agilent HPLC system 1100 Series or 1260 Series (Agilent Technologies, CA, USA California), respectively. Applied columns were an InfinityLab Poroshell 120 EC-C18 (3.0×50 mm; 2.7 micron, Agilent Technologies, CA, USA) or a Kinetex 2.6 μm XB-C18 (100 \AA , 100×4.6 mm, Phenomenex Inc., CA, USA). An overview of applied HPLC and MS/MS parameters can be found in Additional file 2 and Additional file 3, respectively. The data acquisition software was MassLynx (V4.1, Waters, MA, USA).

Quantification of total protein content

The protein content of hCMEC/D3 cells was determined for normalization purposes. Cells were washed with ice-cold phosphate buffered saline following cell lysis in cell extraction buffer (FNN0011, Thermo Fisher Scientific, MA, USA) supplemented with 1×cCompleteTM Protease Inhibitor Cocktail (04693116001, Roche, Basel, Schweiz), 1 mM phenylmethylsulfonyl fluoride, and 1 mg/mL pepstatin for 30 min on ice. The protein concentration was determined using the bicinchoninic acid (BCA) assay kit (bicinchoninic acid and copper (II) sulphate solution) as

directed by the manufacturer. Samples were measured using a SPECTROstar Nano microplate reader (BMG LABTECH, Ortenberg, Germany).

Animals

Male Abcb1a/Abcb1b-eKO1 (P-gp knockout) mice and FVB wild-type counterparts (18–24 g at arrival) were obtained from Shanghai Biomodel Organism Science & Technology Development Co. Ltd (Shanghai, China). Male C57 mice (C57BL/6N) (18–22 g at arrival) were obtained from Beijing Vitalstar Biotechnology Co., Ltd (Beijing, China). Animals were housed in pairs in a temperature-controlled environment (20–24 $^{\circ}\text{C}$) with lighting maintained under a 12-h light–dark cycle. Animals were habituated for at least seven days prior to surgery with free access to food and water. The experiments were carried out in accordance with the Danish legislation regulating animal experiments; Law and Order on Animal experiments; Act No. 1107 of 01/07/2022 and Act No. 1108 of 01/07/2022 and with the specific license for this experiment issued by the National Authority.

In vivo brain distribution by neuropharmacokinetic assessment and equilibrium dialysis

In vivo experiments were conducted to assess the extent of the BBB transport of eletriptan and to elucidate the involvement of active transport processes. All mice were cannulated in the jugular vein for intravenous drug administration. Following surgery, the animals were allowed to recover for 3 days before administration of test compounds. Eletriptan HBr was dosed in P-gp knockout and wild type mice using a loading dose of 2 mg/kg (as bolus) followed by a 2-h constant rate infusion of 3 mg/kg (1.5 mg/kg/h) dissolved in 0.9% NaCl. Diphenhydramine hydrochloride was dosed in C57 mice using a 2-h constant rate infusion of 5 mg/kg (2.5 mg/kg/h) dissolved in 10% HP- β -CD in water. Throughout all studies a dose volume of 10 mL/kg was applied. Serial blood samples were taken from the saphenous vein during the infusion to verify steady state and at the end of infusion. Terminal blood samples were collected from all animals. Brain samples were prepared by homogenization using ultrasonication as described previously [39] and analyzed together with the plasma samples using LC-MS/MS [39]. The lower limit of quantification was determined to 1.0 ng/mL in plasma and 5 ng/g in brain tissue for both eletriptan and diphenhydramine.

Plasma protein and brain tissue binding of eletriptan and diphenhydramine were determined in vitro by equilibrium dialysis using donor test compound solutions of 1 μM incubated in triplicate as described previously [40]. C57 mice were used to prepare blank plasma and brain matrices throughout all binding studies.

The total brain and plasma concentration partition coefficient (K_p) was calculated from Eq. 7.

$$K_p = \frac{C_{\text{tot,brain,ss}}}{C_{\text{tot,plasma,ss}}} \quad (7)$$

where $C_{\text{tot,brain,ss}}$ and $C_{\text{tot,plasma,ss}}$ is the total drug concentration at steady state in brain and plasma, respectively.

The unbound brain and plasma partition coefficient ($K_{p,uu}$) was derived from dividing the unbound brain concentration with the unbound plasma concentration at the end of infusion for each animal. The $K_{p,uu}$ was calculated from Eq. 8.

$$K_{p,uu} = \frac{C_{\text{tot,brain,ss}} \cdot f_{u,\text{brain}}}{C_{\text{tot,plasma,ss}} \cdot f_{u,\text{plasma}}} \quad (8)$$

where $f_{u,\text{brain}}$ and $f_{u,\text{plasma}}$ is the fraction of unbound drug in the brain and plasma, respectively.

Statistical analysis

Statistical analysis was conducted using GraphPad Prism version 9.4.0 (La Jolla, California, USA). Data are presented as mean \pm standard deviation (SD) unless otherwise stated. In vitro experiments were performed in three biological replicates and three technical replicates, unless otherwise stated, where n denotes the number of biological replicates and N_{total} denotes the total number of technical replicates. In vivo experiments were performed in groups of three animals. Statistical analyses were performed by comparing the group means with either two-tailed unpaired Students t-test for comparing two means or by one-way analysis of variance (ANOVA) followed by a Tukey's multiple comparison test for comparison of more than two means. P-values < 0.05 were considered statistically significant.

Results

Physicochemical characteristics of triptans and prototypical H^+ /OC antiporter substrates

Triptans are a relatively homogeneous group of drug compounds with similar physicochemical properties, including molecular weights < 400 g/mol and a low to moderate lipophilicity (cLogD values ranging from -2.1 – 0.18) [41]. Triptans either possess a secondary or a tertiary amine with pK_a values ranging from 8.4 to 10.4, rendering members of this drug class cationic at physiological pH. As a consequence, it is unlikely that triptans cross the brain microvascular endothelium through passive diffusion to a clinically relevant extent. Table 1 summarizes structures and physicochemical properties of the triptans, as well as oxycodone and pyrilamine, which are two prototypical H^+ /OC antiporter substrates included in this study.

The H^+ /OC antiporter was functionally expressed in the hCMEC/D3 cells

The functionality of the H^+ /OC antiporter was probed in the hCMEC/D3 cell line using the prototypical substrates [3H]-pyrilamine and oxycodone. The following criteria were used to confirm functional expression of the H^+ /OC antiporter: (1) Saturable uptake kinetics, (2) competitive inhibition between prototypical H^+ /OC antiporter substrates, and (3) pH-dependent uptake of substrates.

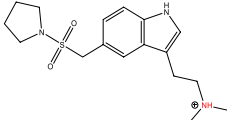
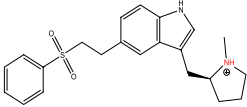
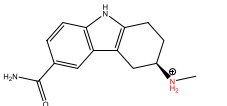
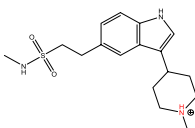
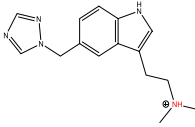
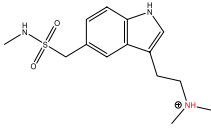
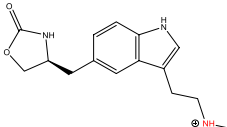
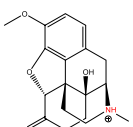
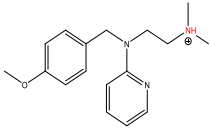
For both [3H]-pyrilamine (Fig. 1A) and oxycodone (Fig. 1B), the time-dependent uptake approached a plateau within a 30-min timeframe. The uptake of [3H]-pyrilamine and oxycodone was reduced by the presence of 500 μM oxycodone and 1000 μM pyrilamine, respectively. We observed concentration-dependent uptake of [3H]-pyrilamine and oxycodone, both revealing saturable uptake kinetics (Fig. 1C and D). The saturable uptake kinetics indicate that the transport is driven by an active uptake mechanism.

The estimated kinetic parameters for [3H]-pyrilamine and oxycodone uptake into the hCMEC/D3 cells are presented in Table 2. The data indicate a slightly higher transporter affinity of pyrilamine (K_m value of ~ 93 μM) as compared to oxycodone (K_m value of ~ 130 μM). No differences were observed in the maximal uptake rate (J_{max}).

The putative H^+ /OC antiporter has been described to function as a proton/drug antiporter [19, 20]. To validate the proton-dependency, the cellular uptake of [3H]-pyrilamine and oxycodone was probed under conditions, where the transmembrane proton gradient was altered by manipulating the intracellular or extracellular pH. Briefly, the uptake of both compounds was affected by manipulating the intracellular and extracellular pH supporting the evidence that these compounds are transported via a proton-driven mechanism, refer Additional file 4. Intracellular alkalization or extracellular acidification resulted in a reduced cellular uptake, while intracellular acidification or extracellular alkalization resulted in an increased cellular uptake, both indicating an oppositely directed proton driving force. Confirmation of intracellular pH changes by NH_4Cl exposure is shown in Additional file 5.

To summarize, the hCMEC/D3 cells revealed characteristics supporting functional expression of the putative H^+ /OC antiporter including saturable uptake kinetics, competitive uptake inhibition, and pH-dependent uptake of known H^+ /OC antiporter substrates. Therefore, the hCMEC/D3 cells were considered a suitable model to investigate the involvement of the H^+ /OC antiporter in brain endothelial cell uptake of triptans.

Table 1 Structures and physicochemical properties of almotriptan, eletriptan, frovatriptan, naratriptan, rizatriptan, sumatriptan, zolmitriptan, oxycodone, and pyrilamine

Compound	Structure pH 7.4	Strongest basic pK _a ^a	Overall charge pH 7.4	Mw (g/mol) ^b	cLogD pH 7.4 ^c
Almotriptan		9.6	Positive	335.5	0.3
Eletriptan		8.4	Positive	382.5	1.1
Frovatriptan		10.4	Positive	243.3	-1.5
Naratriptan		9.2	Positive	335.5	-0.2
Rizatriptan		9.6	Positive	269.3	0.04
Sumatriptan		9.5	Positive	295.4	-0.6
Zolmitriptan		9.6	Positive	287.4	0.4
Oxycodone		8.8	Positive	315.4	0.5
Pyrilamine		8.8	Positive	285.4	1.1

The secondary or tertiary amine is marked in red

^a Extracted from DrugBank® [42]

^b Extracted from PubChem [43]

^c Extracted from ChemSpider [44]

Table 2 Kinetic uptake parameters of prototypical H⁺/OC antiporter substrates, pyrilamine and oxycodone, into hCMEC/D3 cells

Compound	Apparent K _m (μM)	J _{max} (nmol·min ⁻¹ ·mg protein ⁻¹)
Pyrilamine	93 ± 17	5.1 ± 0.7
Oxycodone	130 ± 57	5.3 ± 1.0

Kinetic parameters are represented as mean ± SD (n = 3, N_{total} = 9)**Triptans demonstrated inhibition of [³H]-pyrilamine uptake with IC₅₀ values ranging from 15 to 1729 μM**

To assess the involvement of the H⁺/OC antiporter in the uptake of triptans into endothelial cells, we determined the cellular uptake of the prototypical H⁺/OC antiporter substrate, [³H]-pyrilamine (48 nM), in the presence of

increasing concentrations of the seven different triptans (Fig. 2). We included the H⁺/OC antiporter substrates, non-labelled pyrilamine and oxycodone, as positive controls for uptake inhibition (Fig. 2A and B). The apparent IC₅₀ values are presented in Table 3.

The most prominent triptan-induced inhibition of pyrilamine was observed in the presence of eletriptan (IC₅₀ value of ~15 μM) (Fig. 2C), which was comparable to pyrilamine self-inhibition (IC₅₀ of ~11 μM). Almotriptan exhibited the second most pronounced inhibition of pyrilamine (IC₅₀ value of ~305 μM) (Fig. 2D), a potency comparable to that of oxycodone (IC₅₀ value of ~225 μM). The remaining triptans inhibited the uptake of pyrilamine in the order of naratriptan > rizatriptan > sumatriptan > zolmitriptan > frovatriptan (Fig. 2E-I). An IC₅₀ value could not be obtained for frovatriptan as it did not exhibit sufficient inhibition in the investigated concentration range.

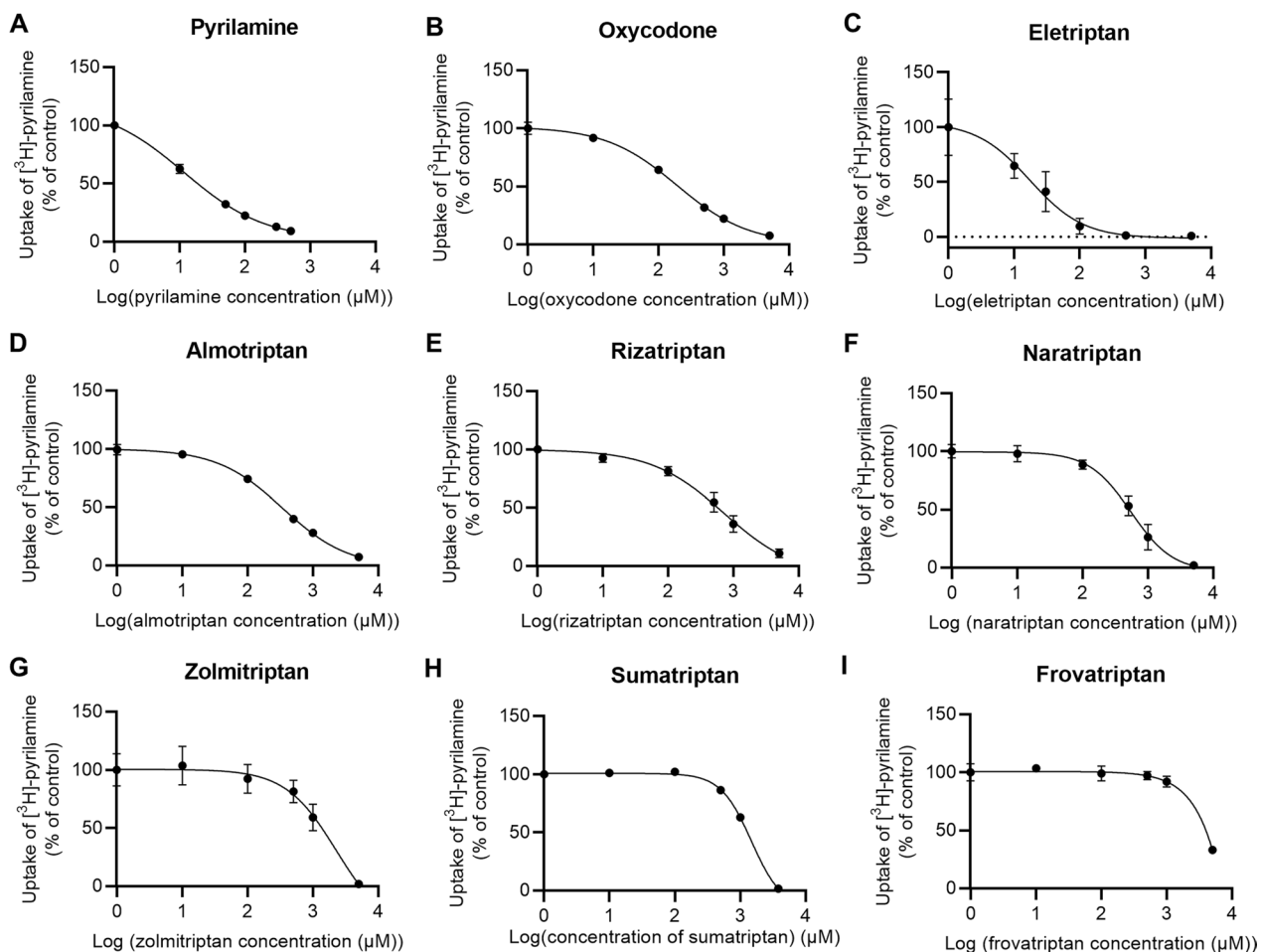
**Fig. 2** Concentration-dependent inhibition of [³H]-pyrilamine uptake into hCMEC/D3 cells. Concentration-dependent inhibition of [³H]-pyrilamine (1 μCi/mL, 48 nM) in the presence of **A** pyrilamine, **B** oxycodone, **C** eletriptan, **D** almotriptan, **E** rizatriptan, **F** naratriptan, **G** zolmitriptan, **H** sumatriptan, and **I** frovatriptan. Note that the logarithm to 0 μM (control) is designated 0 in the figure. Data are fitted to non-linear regression (log(inhibitor) vs. response—Variable slope (four parameters)) (n = 2–3, N_{total} = 6–9). All data points represent mean ± SD

Table 3 Apparent IC₅₀ values on [³H]-pyrilamine uptake (1 μCi/mL, 48 nM) into hCMEC/D3 cells

Compound	Apparent IC ₅₀ (μM)
Pyrilamine	11 ± 6
Oxycodone	225 ± 57
Eletriptan	15 ± 4
Almotriptan	305 ± 83
Naratriptan	460 ± 41
Rizatriptan	719 ± 243
Sumatriptan	1458 ± 189
Zolmitriptan	1729 ± 1209
Frovatriptan	N/A

The IC₅₀ values represent mean ± SD (*n* = 2–3, *N*_{total} = 6–9)

Eletriptan was taken up by hCMEC/D3 cells in a saturable manner

Our inhibition studies indicated that the majority of the triptans competed with pyrilamine for the H⁺/OC antiporter binding site but did not reveal whether they are actual substrates being translocated by the transporter. Three triptans, eletriptan, almotriptan, and sumatriptan, were evaluated as to whether they were transported via the H⁺/OC antiporter in uptake studies using hCMEC/D3 cells and LC-MS/MS for substrate detection. Eletriptan and almotriptan were selected based on their high inhibitory affinity, while sumatriptan was selected based on its poor inhibitory properties.

Eletriptan showed concentration-dependent uptake into hCMEC/D3 cells reaching saturation within a 500 μM concentration (Fig. 3A, Table 4), indicative of carrier-mediated uptake. The H⁺/OC antiporter substrates pyrilamine and oxycodone inhibited the uptake of eletriptan in a statistically significant manner, with the most pronounced inhibition observed in the presence of pyrilamine (Fig. 3B). Almotriptan did not show saturable uptake, but uptake was slightly inhibited in the presence of pyrilamine (Fig. 3C and D). Oxycodone did not inhibit the uptake of almotriptan (Fig. 3D). The uptake of sumatriptan showed a linear increase as function of increasing concentrations (Fig. 3E). Both pyrilamine and oxycodone inhibited the uptake of sumatriptan, with the most pronounced inhibition observed in the presence of oxycodone (Fig. 3F).

Uptake of eletriptan, almotriptan, and sumatriptan in hCMEC/D3 cells were affected by the transmembrane proton gradient

It was evaluated whether eletriptan, almotriptan, and sumatriptan were taken up by hCMEC/D3 cells in a proton-dependent manner, as would be expected from

H⁺/OC antiporter-mediated transport. Cellular uptake of the triptans were performed under conditions where the transmembrane proton gradient was altered through manipulation of the extra- or intracellular pH by acute- or preexposure to 30 mM NH₄Cl (Fig. 4A). The resulting intracellular alkalization or acidification after acute or preexposure to 30 mM NH₄Cl was determined using the fluorescent intracellular probe BCECF, as documented in Additional file 5.

Cellular uptake of eletriptan, almotriptan, and sumatriptan was decreased after intracellular alkalization, caused by acute exposure of the hCMEC/D3 cells to 30 mM NH₄Cl (Fig. 4B–D). Intracellular acidification, caused by pre-exposure to NH₄Cl followed by media change, resulted in a statistically significant increase in the uptake of eletriptan and almotriptan but a decreased uptake of sumatriptan (Fig. 4B–D). Unexpectedly, extracellular acidification (pH 6.8) did not affect eletriptan uptake whereas a slight decrease in eletriptan uptake was observed at pH 8.2 (Fig. 4E). The uptake of both almotriptan (Fig. 4F) and sumatriptan (Fig. 4G) was reduced at pH 6.8 and increased at pH 8.2.

In summary, the uptake of eletriptan, sumatriptan, and almotriptan all showed transmembrane proton gradient dependency in a manner consistent with uptake via a proton antiporter.

Eletriptan displayed P-gp substrate characteristics, i.e. inhibition of digoxin efflux and polarized B-A transport in the IPEC-J2 MDR1 cell line

Our aim was to investigate the mechanisms underlying transport mechanisms of triptans at the BBB. Having established that at least eletriptan showed characteristics of carrier-mediated transport via the H⁺/OC antiporter, we continued to examine whether there was an interaction between the triptans and P-gp, which could potentially lead to triptans being unable to pass the BBB [45, 46]. We screened for potential interactions between the triptans and the prototypical P-gp substrate digoxin using the IPEC-J2 MDR1 cell line [37, 47]. The cellular uptake of [³H]-digoxin (42 nM), was investigated in the absence or presence of eletriptan, sumatriptan, almotriptan, naratriptan, rizatriptan, zolmitriptan, or frovatriptan (500 μM) (Fig. 5A). The specific P-gp inhibitor ZSQ (2 μM) was used as positive control for P-gp inhibition. [³H]-digoxin uptake was increased in a statistically significant manner in the presence of ZSQ (742 ± 308% of control). Likewise, the presence of eletriptan resulted in a statistically significant increase of [³H]-digoxin uptake (222 ± 92% of control), indicating that eletriptan inhibited the P-gp-mediated efflux of [³H]-digoxin. Eletriptan was the only triptan which had an impact on [³H]-digoxin uptake in the IPEC-J2 MDR1 cells.

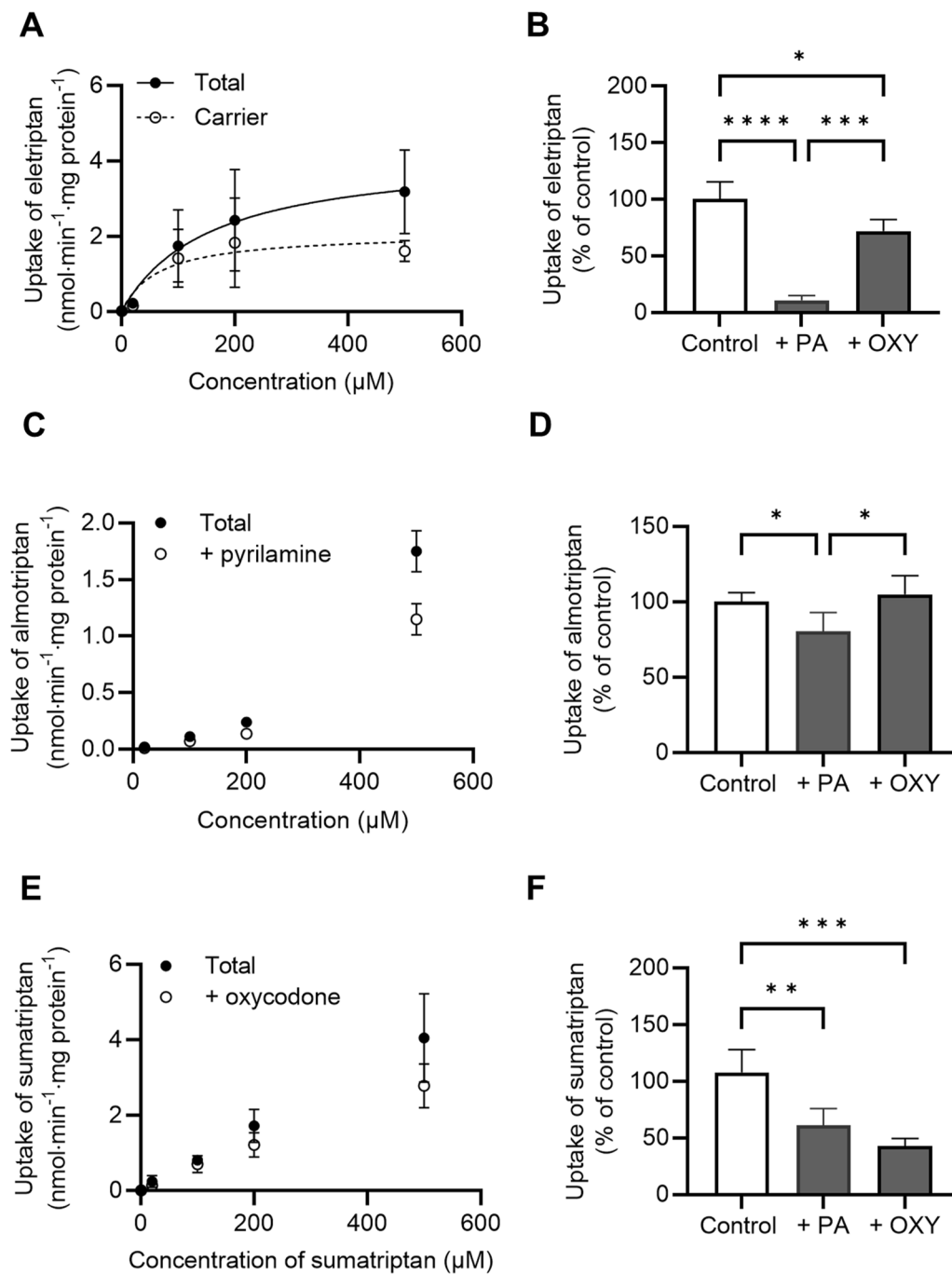


Fig. 3 Uptake properties of eletriptan, almotriptan and sumatriptan into hCMEC/D3 cells. **A** Concentration-dependent uptake of eletriptan in the presence of 1000 μM pyrilamine. The total uptake is shown in closed circles, and the calculated carrier-mediated uptake (total–passive) is shown in open circles. Carrier-mediated uptake is fitted to non-linear regression (Michaelis–Menten kinetics). **B** Uptake of eletriptan (50 μM) in absence (Control) or presence of 500 μM pyrilamine (PA) or 500 μM oxycodone (OXY). **C** Concentration-dependent uptake of almotriptan in the presence of 1000 μM pyrilamine (+pyrilamine). **D** Uptake of almotriptan (50 μM) in absence (Control) or presence of 500 μM pyrilamine (PA) or 500 μM oxycodone (OXY). **E** Concentration-dependent uptake of sumatriptan in the presence of 1000 μM oxycodone (+oxycodone). **F** Uptake of sumatriptan (50 μM) in absence (Control) or presence of 500 μM pyrilamine (PA) or 500 μM oxycodone (OXY). All data points or columns represent *mean ± SD* ($n = 3$, $N_{total} = 9$). Uptake amounts are normalized against protein content per well. Data were analysed using a one-way ANOVA followed by a Tukey's multiple comparison test. *: $P \leq 0.05$. **: $P \leq 0.01$. ***: $P \leq 0.001$. ****: $P \leq 0.0001$

Table 4 Kinetic uptake parameters of eletriptan, almotriptan, and sumatriptan into hCMEC/D3 cells

Compound	Apparent K_m (μM)	J_{max} ($\text{nmol}\cdot\text{min}^{-1}\cdot\text{mg protein}^{-1}$)
Eletriptan	89 ± 38	2.2 ± 0.7
Almotriptan	N/A	N/A
Sumatriptan	N/A	N/A

Kinetic parameters are represented as *mean* ± *SD* ($n=3$, $N_{\text{total}}=9$)

To confirm the notion that eletriptan might be a P-gp substrate, we performed a bidirectional transport study with eletriptan (50 μM) across IPEC-J2 MDR1 monolayers in the absence or presence of ZSQ (2 μM). The TEER across the IPEC-J2 MDR1 monolayers was $1580 \pm 95 \Omega\cdot\text{cm}^2$ ($n=3$, $N_{\text{total}}=36$) prior to the experiments. The apparent permeability (P_{app}) of eletriptan was statistically significant higher in the B to A direction ($2.4 \pm 0.2 \cdot 10^{-5} \text{ cm}\cdot\text{s}^{-1}$) than in the A to B direction ($8.2 \pm 0.5 \cdot 10^{-7} \text{ cm}\cdot\text{s}^{-1}$) (Fig. 5B). Flux curves are shown in Additional

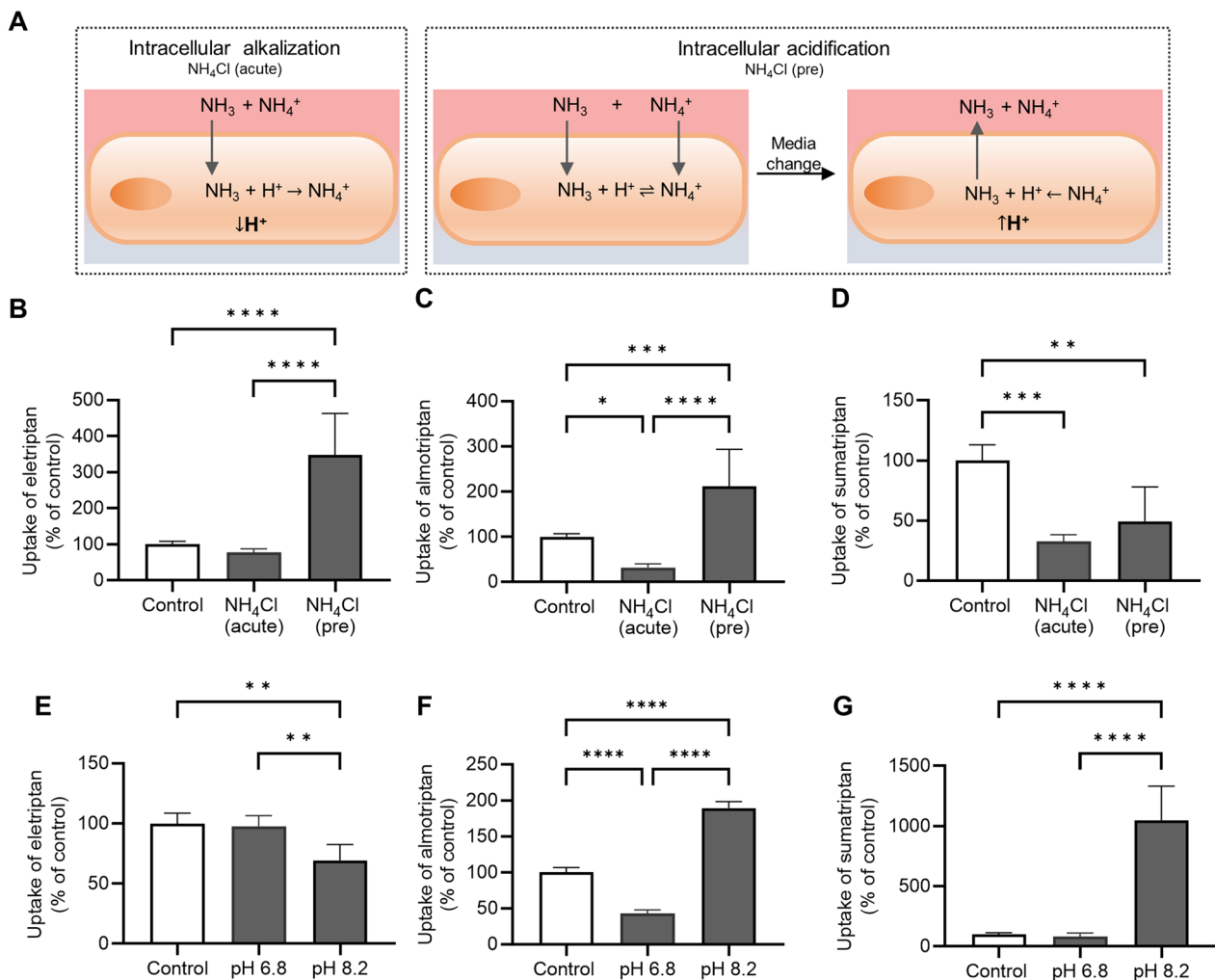


Fig. 4 Cellular uptake of eletriptan, almotriptan and sumatriptan after intra- and extracellular pH manipulation in hCMEC/D3 cells. **A** Schematic representation of intracellular pH changes after acute- or preexposure to 30 mM NH_4Cl . Uncharged NH_3 diffuses into the cells and consumes intracellular protons, consequently leading to intracellular alkalinization. Intracellular acidification will occur upon preexposure to NH_4Cl followed by media change. After 30 min of preexposure to NH_4Cl , both NH_3 and NH_4^+ will enter the cells and reach equilibrium. Upon media change, uncharged NH_3 will quickly diffuse out of the cells causing intracellular accumulation of protons, which will lead to intracellular acidification. **B-D**) Uptake of triptans (500 μM) was investigated in transport buffer pH 7.4 (Control), after acute exposure to NH_4Cl (NH_4Cl (acute)), and after preexposure to NH_4Cl followed by media change (NH_4Cl (pre)). Effect of intracellular pH manipulation on **B** eletriptan uptake, **C** almotriptan uptake, and **D** sumatriptan uptake. **E-G**) Uptake of triptans (500 μM) was investigated in transport buffer with pH 7.4 (Control), pH 6.8 and pH 8.2. Effect on extracellular pH manipulation on **E** eletriptan uptake **F** almotriptan uptake, and **G** sumatriptan uptake. Each column represents *mean* ± *SD* ($n=3$, $N_{\text{total}}=9$). Data were analysed using a one-way ANOVA followed by a Tukey's multiple comparison test. *: $P \leq 0.05$. **: $P \leq 0.01$. ***: $P \leq 0.001$. ****: $P \leq 0.0001$

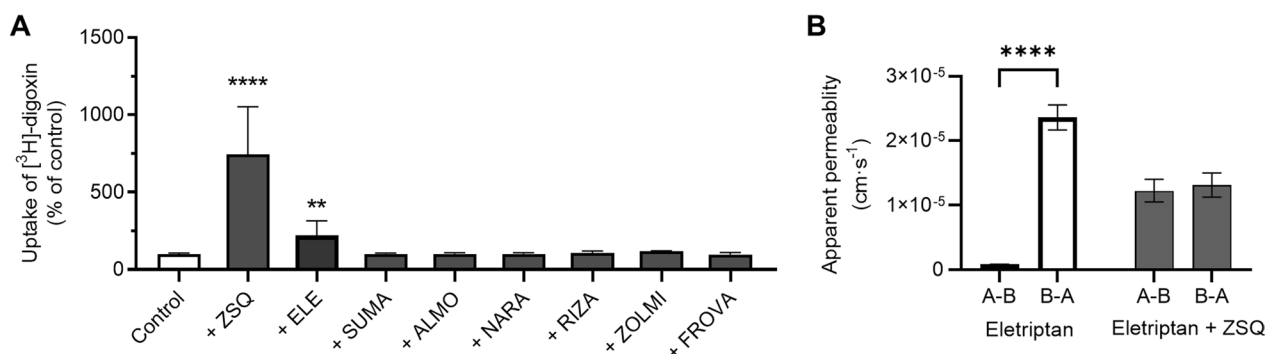


Fig. 5 Triptans interaction with P-gp in IPEC-J2 MDR1 cells. **A** Screening of the inhibitory effects of triptans on [³H]-digoxin uptake into IPEC-MDR1 cells. Uptake of [³H]-digoxin (1 μ Ci/mL, 42 nM) for 15 min in the absence (Control) or presence of 2 μ M zosuquidar (ZSQ), 500 μ M eletriptan (ELE), 500 μ M almotriptan (ALMO), 500 μ M rizatriptan (RIZA), 500 μ M zolmitriptan (ZOLMI), 500 μ M naratriptan (NARA), 500 μ M sumatriptan (SUMA) or 500 μ M frovatriptan (FROVA). Each column represents *mean* \pm *SD* ($n=3$, $N_{total}=9$). Columns were compared to 'Control-group' and analysed using a student's t-test. **: $P \leq 0.01$. ****: $P \leq 0.0001$. **B** Apparent permeabilities (P_{app}) of eletriptan (50 μ M) in the absence or presence of ZSQ (2 μ M) in the A-B or B-A direction. Each column represents *mean* \pm *SD* ($n=3$, $N_{total}=9$). Data were analysed using a two-way ANOVA followed by a Tukey's multiple comparison test. ****: $P \leq 0.0001$

file 6. The efflux ratio (ER) for eletriptan was calculated to be 28.9 ± 1.8 , thus demonstrating active efflux. The polarized bidirectional transport of eletriptan was completely abolished in the presence of ZSQ ($P_{app,A-B}$ $1.2 \pm 0.2 \cdot 10^{-5}$ $\text{cm}\cdot\text{s}^{-1}$ and $P_{app,B-A}$ $1.3 \pm 0.2 \cdot 10^{-5}$ $\text{cm}\cdot\text{s}^{-1}$), which reduced the ER close to unity (1.1 ± 0.1). These results further show that eletriptan is a substrate of the P-gp efflux pump.

Eletriptan brain-to-plasma distribution in wild type and *mdr1a/1b* knockout mice indicated that active carrier-mediated uptake and P-gp-mediated efflux occurs simultaneously at the BBB

After having established that eletriptan showed both uptake properties in hCMEC/D3 cells consistent with eletriptan being a H⁺/OC antiporter substrate, and P-gp mediated efflux in IPEC-J2 MDR1 cells, we proceeded to investigate the brain uptake of eletriptan in vivo. The total and unbound brain-to-plasma partitioning coefficients (K_p and $K_{p,uu}$) were determined in wild type and *mdr1a/1b* knockout mice at steady state using the combinatory mapping approach [48]. We included the H⁺/OC antiporter substrate diphenhydramine, as a positive control for active uptake via the H⁺/OC antiporter [31]. Steady state conditions were achieved after a bolus dose followed by a 2-h constant infusion giving plasma concentrations of 259 ± 30 ng/mL. The rationale for selecting this dosing regimen was to obtain a constant plasma concentration that is relatively compatible with clinically relevant human peak plasma concentrations of 94–200 ng/mL [3]. Steady state conditions were achieved after a 2-h constant infusion rate (Fig. 6A). We observed low total brain concentrations of eletriptan in wild type mice, but

the concentration rose drastically in *mdr1a/1b* knockout mice supporting the role of P-gp keeping eletriptan out of the brain (Fig. 6B). K_p and $K_{p,uu}$ for eletriptan and diphenhydramine are shown in (Fig. 6C and D). In wild type mice, we observed a K_p of 0.17 and a $K_{p,uu}$ of 0.04 for eletriptan, which was increased in a statistically significant manner in *mdr1a/1b* knockout mice to a K_p and $K_{p,uu}$ of 6.35 and 1.32 (>30-fold increase), respectively. The positive control for active uptake via the H⁺/OC antiporter, diphenhydramine, yielded a K_p and a $K_{p,uu}$ of 9.20 and 1.72, respectively. A summary of the determined free fractions (f_u) and neuropharmacokinetic parameters is shown in Table 5.

Discussion

The novelty of the present study is that the triptan family of compounds possesses affinity for the H⁺/OC antiporter, a BBB transport mechanism. At least eletriptan was shown to be a novel substrate of this transporter. In vivo, eletriptan accumulated in the brain when the P-gp function was absent, also indicating active uptake via the H⁺/OC antiporter.

Triptans are a novel group of compounds shown to interact with the H⁺/OC antiporter

The scope of the study was to investigate possible mechanisms for triptan transport across the BBB and evaluate whether the H⁺/OC antiporter and P-gp contributed to brain uptake and efflux, respectively. Except for frovatriptan, all triptans demonstrated an inhibitory effect on the H⁺/OC antiporter with IC_{50} values ranging from 15 to 1729 μ M. Eletriptan displayed the greatest inhibitory potency on pyrilamine uptake among the different

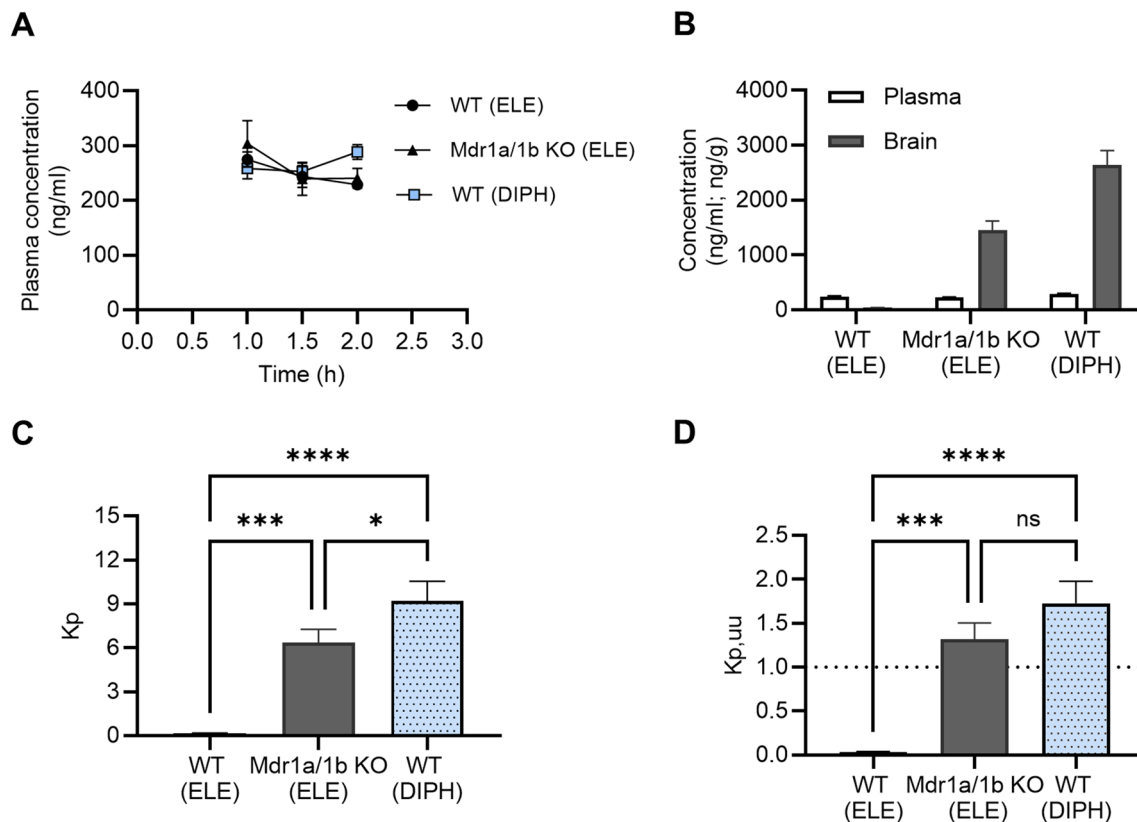


Fig. 6 Neuropharmacokinetic assessment of eletriptan and diphenhydramine in wild type (WT) and *mdr1a/1b* knockout (KO) mice at steady state. **A** Plasma time-concentration profiles of eletriptan in wild type mice (WT (ELE)), *mdr1a/1b* knockout mice (*Mdr1a/1b* KO (ELE)), or diphenhydramine in wild type mice (WT (DIPH)) during a 2-h constant intravenous infusion. **B** Total concentrations of eletriptan and diphenhydramine in plasma or brain at steady state. **C** Total brain-to-plasma partitioning coefficient (K_p). **D** Unbound brain-to-plasma partitioning coefficient ($K_{p,uu}$). The dotted line represents the $K_{p,uu}$ of unity. All data points or columns represent $mean \pm SD$ ($n=3$). Data were analysed using a one-way ANOVA followed by a Tukey's multiple comparison test. *: $P \leq 0.05$. ***: $P \leq 0.001$. ****: $P \leq 0.0001$

Table 5 Neuropharmacokinetic parameters of eletriptan and diphenhydramine in wild type and *mdr1a/1b* knockout mice

Parameters	Unit	Eletriptan		Diphenhydramine
		Wild type	<i>mdr1a/1b</i> knockout	Wild type
$f_{u,plasma}$	%	40	40	40
$f_{u,brain}$	%	8.3	8.3	7.5
$C_{,plasma}$	ng/mL	240 ± 18	229 ± 6	288 ± 14
$C_{,brain}$	ng/mL	41 ± 5	1448 ± 175	2640 ± 265
$K_p (C_{,brain}/C_{,plasma})$	unitless	0.17 ± 0.016	6.35 ± 0.91	9.20 ± 1.35
$K_{p,uu} (C_{,brain} \cdot f_{u,brain})/C_{,plasma} \cdot f_{u,plasma}$	unitless	0.04 ± 0.004	1.32 ± 0.19	1.72 ± 0.25

Data are represented as $mean \pm SD$ ($n=3$)

triptans, thus indicating the strongest H^+ /OC antiporter interaction. Additionally, eletriptan uptake could almost be completely inhibited in the presence of the prototypical substrate, pyrilamine. The potent inhibitory potential of eletriptan on pyrilamine uptake and vice versa, further point towards that these two compounds represent ideal

competitive model substrates for future investigations of the H^+ /OC antiporter. The demonstrated uptake properties of the three investigated triptans, eletriptan, almotriptan, and sumatriptan are summarized in Table 6.

Eletriptan displayed saturable uptake kinetics into hCMEC/D3 cells, while the cellular uptake of

Table 6 Overview of the demonstrated uptake properties of eletriptan, almotriptan and sumatriptan into hCMEC/D3 cells

	Eletriptan	Almotriptan	Sumatriptan
IC ₅₀ value on pyrillamine uptake	IC ₅₀ = 15 ± 4 μM	IC ₅₀ = 305 ± 83 μM	IC ₅₀ = 1458 ± 189 μM
K _m value	K _m = 89 ± 38 μM	not saturable (in tested range)	not saturable (in tested range)
Inhibition by oxycodone #	yes (*)	no	yes (***)
Inhibition by pyrillamine #	yes (****)	yes (*)	yes (**)
Proton-gradient dependence	yes	yes	yes
Association with H ⁺ /OC antiporter	Substrate potent inhibitor	(substrate) decent inhibitor	(substrate) very poor inhibitor

Uptake of the triptans in the absence or presence of oxycodone or pyrillamine were compared using a one-way ANOVA followed by a Tukey's multiple comparison test

*: P ≤ 0.05. **: P ≤ 0.01. ***: P ≤ 0.001. ****: P ≤ 0.0001

almotriptan and sumatriptan revealed no saturation at the tested concentration range. Eletriptan, almotriptan, and sumatriptan uptake were driven by a proton-dependent mechanism, which could indicate the involvement of the H⁺/OC antiporter. In addition to changing the proton driving force of a potential transporter, pH manipulation also affects the protonation degree of the compounds (pK_a 8.4–9.6, refer Table 1). Changing the protonation degree of the triptans may affect their passive diffusion properties as well as their affinity towards the transporter, since a protonated amine moiety has shown to be essential for the H⁺/OC antiporter recognition [20, 33]. Thus, the data from the extracellular pH manipulation experiments must be interpreted with caution (Fig. 4). However, as intracellular pH manipulation also showed a tendency towards a pH-dependent uptake mechanism, we expect changes to the observed uptake of eletriptan, almotriptan, and sumatriptan to be a result of the proton gradient and not solely due to changes in the protonation degree of the triptans.

At least eletriptan was found to be a novel substrate for the H⁺/OC antiporter in the present study, while almotriptan, sumatriptan, rizatriptan, naratriptan, and zolmitriptan showed inhibitory affinity towards the transporter.

In agreement with our findings, Doetsch et al. [49] recently proposed that eletriptan might be a substrate of the H⁺/OC antiporter based on in vitro trans-stimulation screening in hCMEC/D3 cells using diphenhydramine as a H⁺/OC antiporter substrate [49]. Frovatriptan and zolmitriptan were also included in that study but did not appear to be H⁺/OC antiporter substrate candidates [49]. Doetsch et al. further evaluated whether eletriptan, frovatriptan, and zolmitriptan were substrates of the organic cation transporter 1 (OCT1). Their findings suggested that frovatriptan and zolmitriptan were substrates of OCT1, while eletriptan was not [49]. In addition, Cheng et al. (2012) have

suggested the organic anion-transporting polypeptide 1A2 (OATP1A2) as a carrier with the potential to transport triptans across the BBB [50].

Eletriptan undergoes simultaneous active uptake and active efflux across the BBB

In the present study, we only identified eletriptan as a P-gp substrate among the triptan family. However, other members of the triptan family have previously been identified as P-gp substrates [51–53]. In the present study, we demonstrated an ER of 28.9 ± 1.8 for eletriptan in IPEC-J2 MDR1 cells. Mahar et al. [53] have previously identified eletriptan (ER of 44.7) and zolmitriptan (ER of 2.48) to be P-gp substrates in the MDR1-transfected Madin Darby canine kidney type II (MDR1-MDCKII) cell line, whereas sumatriptan was not [53]. Additionally, Wilt et al. [51] demonstrated P-gp-mediated efflux of eletriptan and sumatriptan, most pronounced for eletriptan, using indirect measurement of ATP hydrolysis in P-gp-integrated liposomes from wild type mice [51]. Evans et al. [52] assessed the in vivo brain K_p in wild type and *mdr1a* knockout mice for sumatriptan, zolmitriptan, naratriptan, rizatriptan, and eletriptan [52]. Their findings revealed that rizatriptan, naratriptan, and eletriptan were indeed substrates of P-gp, while sumatriptan and zolmitriptan were not.

As demonstrated in the present study, eletriptan underwent active uptake and active efflux in hCMEC/D3 and IPEC-J2 MDR1 cells, respectively. We evaluated this two-way transport phenomenon mediated by two distinct transporters in vivo in both wild type and *mdr1a/1b* knockout mice. We demonstrated low brain uptake of eletriptan in wild type mice, but with a drastically higher uptake in *mdr1a/1b* knockout mice (> 30-fold increase), which clearly imply P-gp involvement. Eletriptan demonstrated a K_{p,uu} higher than unity (1.32) in *mdr1a/1b* knockouts indicating an active uptake mechanism at the BBB. The active uptake component was completely abolished by P-gp in wild type mice indicating poor

permeation properties or dominating efflux across the BBB.

The fact that the free brain concentration of eletriptan increased to values higher than the free plasma concentration in the *mdr1a/1b* knockout mice indicated that (1) eletriptan have a high baseline permeability across the BBB in the absence of the P-gp function, and (2) P-gp is instrumental in keeping brain eletriptan concentrations low in wild type mice. The eletriptan $K_{p,uu}$ values above unity also supported that the high baseline permeability is due to an energy-dependent transporter since an uphill concentration gradient is maintained. This was confirmed by comparing eletriptan $K_{p,uu}$ with the control substrate diphenhydramine.

Diphenhydramine was included as a positive control for active uptake via the H^+/OC antiporter. Previous microdialysis studies in rats, have reported $K_{p,uu}$ values between 3.24–5.5 for diphenhydramine, which clearly indicate active uptake across the BBB [30–32]. In our study design, where we estimate $K_{p,uu}$ in experiments on mice, using the K_p value and calculated free concentrations, diphenhydramine displayed a $K_{p,uu}$ of 1.72. Although the values differ somewhat, they are indicative of H^+/OC antiporter-mediated active uptake. The differences may be due to species, or a methodological bias. Eletriptan did also display accumulation ($K_{p,uu}$ of 1.32) in the parenchyma in the knock-out mice where the P-gp function was absent. Our *in vitro* and *in vivo* findings support the notion that eletriptan is subjected to simultaneous influx and efflux, likely facilitated by the putative H^+/OC antiporter and P-gp.

Clinical implications

Inhibition of pyrilamine uptake differed substantially among the triptans, not reflecting the apparent homogeneity in physicochemical properties (Table 1 and Additional file 7). However, triptans also exhibit marked differences in their clinical efficacy and tolerability profiles within and among patients [8, 54]. We show that the affinity for both the H^+/OC antiporter and the P-gp efflux pump seems to differ considerably among the triptans (Figs. 2 and 5A). This observation could potentially provide some explanation on the documented differences in clinical efficacy and tolerability. Furthermore, our findings emphasize the potential of transporter-related drug-drug interactions, when co-administering triptans with substrates of either the H^+/OC antiporter or P-gp. However, the apparent K_m of eletriptan found in hCMEC/D3 cells is much higher than clinically relevant plasma concentrations (246–523 nM) [3]. This may indicate that eletriptan is not saturating the H^+/OC antiporter *in vivo* and is therefore not likely to cause transporter associated drug-drug interactions.

Further studies are essential to determine to what extent triptans enter the brain at clinically relevant concentrations and elucidate triptans potential of initiating a central $5HT_{1B/1D}$ receptor-mediated response. A previous study conducted by Deen et al. [11] demonstrated that the administration of sumatriptan in humans resulted in a notable reduction in central $5HT_{1B}$ receptor binding. This outcome suggests that sumatriptan exert a pharmacological effect in the brain [11]. Whether central $5HT_{1B/1D}$ receptor activation leads to anti-migraine and/or potential side effects are still to be elucidated.

Conclusions

The present study explored the involvement of the putative H^+/OC antiporter and the P-gp efflux pump in BBB transport of seven clinically relevant triptans. To our knowledge, we are the first to demonstrate that the triptan family of compounds possesses affinity for the H^+/OC antiporter. We propose that the putative H^+/OC antiporter might play a role in the BBB transport of some triptans, particularly eletriptan. We confirmed previous studies showing that eletriptan is a substrate of P-gp. Neuropharmacokinetic assessment of eletriptan demonstrated low brain uptake in wild type mice but with a drastically increased uptake in *mdr1a/1b* knockouts. These findings suggest that eletriptan is subject to simultaneous brain uptake and efflux, possibly facilitated by the putative H^+/OC antiporter and P-gp, respectively.

In conclusion, this study sheds light on the involvement of the H^+/OC antiporter and P-gp for brain parenchymal uptake of triptans at the BBB level. These findings may contribute to a better understanding of the ability of triptans to bear a central site of action as well as emphasizing potential transporter-related drug-drug interactions.

Abbreviations

$5HT_{1B/1D}$ receptor	5-Hydroxytryptamine receptor 1B/1D
A-B	Apical-to-basolateral
B-A	Basolateral-to-apical
BBB	Blood–brain barrier
BCECF-AM	2',7'- Bis-(Carboxyethyl)-5(6')-carboxyfluorescein acetoxymethyl ester
BSA	Bovine serum albumin
CNS	Central nervous system
ER	Efflux ratio
FBS	Fetal bovine serum
$f_{u,plasma}$	Free fraction in plasma
$f_{u,brain}$	Free fraction in brain
HBSS	Hank's balanced salt solution
hCMEC/D3	Human cerebral microvascular endothelial cell line D3
HEPES	N-2-hydroxyethylpiperazine-N-2-ethane sulfonic acid
H^+/OC antiporter	Proton-coupled organic cation antiporter
IC_{50}	Inhibitory constant at 50% inhibition
IPEC-J2	Intestinal porcine epithelial cell line J2
J_{max}	Maximal uptake flux
K_m	Michaelis Menten constant
KO	Knockout
K_p	Total brain-to-total plasma concentration ratio

$K_{p,uu}$	Unbound brain-to-unbound plasma concentration ratio
MDCKII	Madin Darby canine kidney type II
MDR1	Human gene encoding P-gp
mdr1a/1b	Rodent gene encoding P-gp
NH ₄ Cl	Ammonium chloride
OATP1A2	Organic anion-transporting polypeptide 1A2
OCT1	Organic cation transporter 1
Papp	Apparent permeability
P-gp	P-glycoprotein
SD	Standard deviation
SEM	Standard error of mean
TEER	Trans epithelial electrical resistance
WT	Wild type
ZSQ	Zosuquidar

Supplementary Information

The online version contains supplementary material available at <https://doi.org/10.1186/s12987-024-00544-6>.

Additional file 1: Time-dependent uptake of eletriptan and almotriptan into hCMEC/D3 cells. **A** Time-dependent uptake of eletriptan (50 μ M) in the absence (Control) or presence of 1000 μ M pyrillamine (+pyrillamine) *mean* \pm *SEM* ($n = 4$, $N_{total} = 12$). **B** Time-dependent uptake of almotriptan (500 μ M) in the absence (Control) or presence of 1000 μ M pyrillamine (+pyrillamine). Uptake amounts are normalized to protein amount per well. Each data point represents *mean* \pm *SD* ($n = 3$, $N_{total} = 9$).

Additional file 2: HPLC parameters for almotriptan, eletriptan, sumatriptan, and oxycodone.

Additional file 3: MS/MS conditions for almotriptan, eletriptan, sumatriptan, and oxycodone.

Additional file 4: Cellular uptake of the prototypical H⁺/OC antiporter substrates, [³H]-pyrillamine and oxycodone, after intra- and extracellular pH manipulation in hCMEC/D3 cells. **A** Effect of intracellular pH manipulation on [³H]-pyrillamine uptake. Uptake of [³H]-pyrillamine (1 μ Ci/mL, 48 nM) was investigated in transport buffer pH 7.4 (Control), after acute exposure to NH₄Cl (NH₄Cl (acute)), and after preexposure to NH₄Cl followed by media change (NH₄Cl (pre)). **B** Effect of intracellular pH manipulation on oxycodone uptake. Uptake of oxycodone (500 μ M) was investigated in transport buffer pH 7.4 (Control), after acute exposure to NH₄Cl (NH₄Cl (acute)), and after preexposure to NH₄Cl followed by media change (NH₄Cl (pre)). **C** Effect on extracellular pH manipulation on [³H]-pyrillamine uptake. Uptake of [³H]-pyrillamine (1 μ Ci/mL, 48 nM) was investigated in transport buffer with pH 7.4 (Control), pH 6.8 and pH 8.2 **D** Effect on extracellular pH manipulation on oxycodone uptake. Uptake of oxycodone (500 μ M) was investigated in transport buffer with pH 7.4 (Control), pH 6.8 and pH 8.2. Each column represents *mean* \pm *SD* ($n = 3$, $N_{total} = 9$). Data were analyzed using a one-way ANOVA followed by a Tukey's multiple comparison test. **: $P \leq 0.01$. ***: $P \leq 0.001$. ****: $P \leq 0.0001$.

Additional file 5: Intracellular pH measurements using BCECF-AM probe. **A** Schematic illustration of BCECF-AM as pH indicator. The cell permeable BCECF-AM enters the cells, where BCECF-AM will undergo hydrolysis to the impermeable BCECF. Fluorescence signal at excitation wavelength of 480 and an emission wavelength of 520 (Ex480/Em520) depends on intracellular pH. An increase in intracellular pH will increase the fluorescent signal, whereas a decrease in intracellular pH will reduce the fluorescent signal. **B** Fluorescent microscopy of BCECF-AM loaded hCMEC/D3 cells. The BCECF-AM dye was loaded in concentrations of 0, 0.5, 1, and 5 μ M. Scale bar represents 100 μ m. ($n = 1$) **C-D** Changes in intracellular pH were measured over time in BCECF-AM- loaded hCMEC/D3 cells (5 μ M) after **C** acute administration of 30 mM NH₄Cl. 30 mM NH₄Cl was added automatically after 15 seconds baseline measurements or **D** preincubation with NH₄Cl in 30-60 minutes followed by manual buffer change to hHBSS(-) without NH₄Cl. No buffer change control represents the baseline. ($n = 3$, $N_{total} = 9$). Each data point represents *mean* \pm *SD*.

Additional file 6: Flux curves of eletriptan across IPEC-J2 MDR1 monolayers. The accumulated amounts of eletriptan (50 μ M) in the absence or presence of ZSQ (2 μ M) in the receiver chamber from apical to basolateral

compartment (A–B) or basolateral to apical compartment (B–A). Each data point represents *mean* \pm *SD* ($n = 3$, $N_{total} = 9$).

Additional file 7: Screening of triptans inhibitory effect on [³H]-pyrillamine uptake into hCMEC/D3 cells. **A** Uptake of [³H]-pyrillamine (48 nM) in the absence (Control) or presence of 500 μ M oxycodone (OXY), eletriptan (ELE), almotriptan (ALMO), rizatriptan (RIZA), zolmitriptan (ZOLMI), naratriptan (NARA), sumatriptan (SUMA) or frovatriptan (FROVA). Each column represents *mean* \pm *SD* ($n = 3$, $N_{total} = 9$). Columns were compared to 'Control-group' and analysed using a one-way ANOVA followed by a Tukey's multiple comparison test. *: $P \leq 0.05$. ***: $P \leq 0.001$. ****: $P \leq 0.0001$.

Acknowledgements

The authors would like to acknowledge Mette Frandsen for culturing IPEC-J2 MDR1 cells used in this study. We would also like to acknowledge Bente Gammelgaard and Camilla Jensen for their assistance in setting up LC-MS/MS methods.

Author contributions

NS, ABV, and AR conducted experimental work and data treatment. CB designed the in vivo studies. NS, ABV, AR, BO, LS, MK, CB, and BB participated in the experimental design and data analysis. PTH and BB were involved with study conceptualization. NS drafted the initial version of the manuscript. All authors participated in finalizing the manuscript and approved the final version of the manuscript.

Funding

Open access funding provided by Copenhagen University. The authors would like to thank Helene and Viggo Bruuns foundation for supporting this study.

Availability of data and materials

All data generated or analyzed during this study are included in this published article and its supplementary information files.

Declarations

Ethics approval and consent to participate

All animal work was carried out in accordance with the national legislations regulating animal experiments in China and Denmark.

Consent for publication

Not applicable.

Competing interests

The authors declare that they have no competing interests.

Author details

¹Department of Pharmacy, University of Copenhagen, Copenhagen, Denmark. ²Biotherapeutic Discovery, H. Lundbeck A/S, Valby, Denmark. ³Bioneer: FARMA, Bioneer A/S, Copenhagen, Denmark. ⁴Translational DMPK, H. Lundbeck A/S, Valby, Denmark. ⁵Danish Headache Center, Department of Neurology, Rigshospitalet-Glostrup, University of Copenhagen, Glostrup, Denmark.

Received: 13 March 2024 Accepted: 25 April 2024

Published online: 06 May 2024

References

- Ashina M, Katsarava Z, Do TP, Buse DC, Pozo-Rosich P, Özge A, et al. Migraine: epidemiology and systems of care. *Lancet*. 2021;397(10283):1485–95.
- Amiri P, Kazeminasab S, Nejadghaderi SA, Mohammadinasab R, Pourfathi H, Araj-Khodaei M, et al. Migraine: a review on its history, global epidemiology, risk factors, and comorbidities. *Front Neurol*. 2021;12:800605.
- de Vries T, Villalon CM, MaassenVanDenBrink A. Pharmacological treatment of migraine: CGRP and 5-HT beyond the triptans. *Pharmacol Ther*. 2020;211:107528.

4. Benemei S, Cortese F, Labastida-Ramirez A, Marchese F, Pellesi L, Romoli M, et al. Triptans and CGRP blockade—impact on the cranial vasculature. *J Headache Pain*. 2017;18(1):103.
5. de Vries T, Villalón CM, MaassenVanDenBrink A. Pharmacological treatment of migraine: CGRP and 5-HT beyond the triptans. *Pharmacol Ther*. 2020;211:107528.
6. Cottier KE, Vanderah TW, Largent-Milnes TM. The CNS as a primary target for migraine therapeutics. *Curr Topics Pharmacol*. 2017;21:1–16.
7. Tfelt-Hansen PC. Does sumatriptan cross the blood-brain barrier in animals and man? *J Headache Pain*. 2010;11(1):5–12.
8. Dodick DW, Martin V. Triptans and CNS side-effects: pharmacokinetic and metabolic mechanisms. *Cephalalgia*. 2004;24(6):417–24.
9. Ferrari MD, Goadsby PJ, Roon KI, Lipton RB. Triptans (serotonin, 5-HT_{1B/1D} agonists) in migraine: detailed results and methods of a meta-analysis of 53 trials. *Cephalalgia*. 2002;22(8):633–58.
10. Muzzi M, Zecchi R, Ranieri G, Urru M, Tofani L, De Cesaris F, et al. Ultra-rapid brain uptake of subcutaneous sumatriptan in the rat: Implication for cluster headache treatment. *Cephalalgia*. 2019;40(4):330–6.
11. Deen M, Hougaard A, Hansen HD, Schain M, Dyssegaard A, Knudsen GM, et al. Association between Sumatriptan treatment during a migraine attack and central 5-HT_{1B} Receptor Binding. *JAMA Neurol*. 2019;76(7):834–40.
12. Varnäs K, Jučaitė A, McCarthy DJ, Stenkrona P, Nord M, Halldin C, et al. A PET study with [¹¹C]AZ10419369 to determine brain 5-HT_{1B} receptor occupancy of Zolmitriptan in healthy male volunteers. *Cephalalgia*. 2013;33(10):853–60.
13. Sakai Y, Dobson C, Diksic M, Aubé M, Hamel E. Sumatriptan normalizes the migraine attack-related increase in brain serotonin synthesis. *Neurology*. 2008;70(6):431–9.
14. Wall A, Kågedal M, Bergström M, Jacobsson E, Nilsson D, Antoni G, et al. Distribution of Zolmitriptan into the CNS in healthy volunteers. *Drugs R D*. 2005;6(3):139–47.
15. Dobson CF, Tohyama Y, Diksic M, Hamel E. Effects of acute or chronic administration of anti-migraine drugs Sumatriptan and Zolmitriptan on serotonin synthesis in the rat brain. *Cephalalgia*. 2004;24(1):2–11.
16. Johnson DE, Rollema H, Schmidt AW, McHarg AD. Serotonergic effects and extracellular brain levels of eletriptan, zolmitriptan and sumatriptan in rat brain. *Eur J Pharmacol*. 2001;425(3):203–10.
17. Goldberg MJ, Spector R, Chiang CK. Transport of diphenhydramine in the central nervous system. *J Pharmacol Exp Ther*. 1987;240(3):717–22.
18. Yamazaki M, Fukuko H, Nagata O, Kato H, Ito Y, Terasaki T, et al. Transport mechanism of an H₁-antagonist at the blood-brain barrier: transport mechanism of mepyramine using the carotid injection technique. *Biol Pharm Bull*. 1994;17(5):676–9.
19. Okura T, Hattori A, Takano Y, Sato T, Hammarlund-Udenaes M, Terasaki T, et al. Involvement of the pyrilamine transporter, a putative organic cation transporter, in blood-brain barrier transport of oxycodone. *Drug Metab Dispos*. 2008;36(10):2005–13.
20. Sachkova A, Jensen O, Dückler C, Ansari S, Brockmüller J. The mystery of the human proton-organic cation antiporter: one transport protein or many? *Pharmacol Ther*. 2022;239:108283.
21. Shimomura K, Okura T, Kato S, Couraud PO, Schermann JM, Terasaki T, et al. Functional expression of a proton-coupled organic cation (H⁺/OC) antiporter in human brain capillary endothelial cell line hCMEC/D3, a human blood-brain barrier model. *Fluids Barriers CNS*. 2013;10(1):8.
22. Kurosawa T, Tega Y, Uchida Y, Higuchi K, Tabata H, Sumiyoshi T, et al. Proteomics-based transporter identification by the PICK method: involvement of TM7SF3 and LHFPL6 in proton-coupled organic cation antiporter at the blood-brain barrier. *Pharmaceutics*. 2022. <https://doi.org/10.3390/pharmaceutics14081683>.
23. Kubo Y, Kusagawa Y, Tachikawa M, Akanuma S, Hosoya K. Involvement of a novel organic cation transporter in verapamil transport across the inner blood-retinal barrier. *Pharm Res*. 2013;30(3):847–56.
24. Kurosawa T, Tega Y, Higuchi K, Yamaguchi T, Nakakura T, Mochizuki T, et al. Expression and functional characterization of drug transporters in brain microvascular endothelial cells derived from human induced pluripotent stem cells. *Mol Pharmaceut*. 2018;15(12):5546–55.
25. Kitamura A, Higuchi K, Okura T, Deguchi Y. Transport characteristics of tramadol in the blood-brain barrier. *J Pharm Sci*. 2014;103(10):3335–41.
26. Higuchi K, Kitamura A, Okura T, Deguchi Y. Memantine transport by a proton-coupled organic cation antiporter in hCMEC/D3 cells, an in vitro human blood-brain barrier model. *Drug Metab Pharmacokin*. 2015;30(2):182–7.
27. Okura T, Ito R, Ishiguro N, Tamai I, Deguchi Y. Blood-brain barrier transport of pramipexole, a dopamine D2 agonist. *Life Sci*. 2007;80(17):1564–71.
28. Tega Y, Akanuma S, Kubo Y, Terasaki T, Hosoya K. Blood-to-brain influx transport of nicotine at the rat blood-brain barrier: involvement of a pyrilamine-sensitive organic cation transport process. *Neurochem Int*. 2013;62(2):173–81.
29. Kurosawa T, Higuchi K, Okura T, Kobayashi K, Kusuhara H, Deguchi Y. Involvement of proton-coupled organic cation antiporter in varenicline transport at blood-brain barrier of rats and in human brain capillary endothelial cells. *J Pharm Sci*. 2017;106(9):2576–82.
30. Kawase A, Chuma T, Irie K, Kazaoka A, Kakuno A, Matsuda N, et al. Increased penetration of diphenhydramine in brain via proton-coupled organic cation antiporter in rats with lipopolysaccharide-induced inflammation. *Brain Behav Immunity Health*. 2021. <https://doi.org/10.1016/j.bbih.2020.100188>.
31. Sadiq MW, Borgs A, Okura T, Shimomura K, Kato S, Deguchi Y, et al. Diphenhydramine active uptake at the blood-brain barrier and its interaction with oxycodone in vitro and in vivo. *J Pharm Sci*. 2011;100(9):3912–23.
32. Kitamura A, Okura T, Higuchi K, Deguchi Y. Cocktail-dosing microdialysis study to simultaneously assess delivery of multiple organic-cationic drugs to the brain. *J Pharm Sci*. 2016;105(2):935–40.
33. Smirnova MA, Goracci L, Cruciani G, Federici L, Declèves X, Chapy H, et al. Pharmacophore-based discovery of substrates of a novel drug/proton-antiporter in the human brain endothelial hCMEC/D3 cell line. *Pharmaceutics*. 2022. <https://doi.org/10.3390/pharmaceutics14020255>.
34. Chapy H, Goracci L, Vayer P, Parmentier Y, Carrupt P-A, Declèves X, et al. Pharmacophore-based discovery of inhibitors of a novel drug/proton antiporter in human brain endothelial hCMEC/D3 cell line. *Brit J Pharmacol*. 2015;172:4888–904.
35. Chapy H, Smirnova M, Andre P, Schlatter J, Chiadmi F, Couraud PO, et al. Carrier-mediated cocaine transport at the blood-brain barrier as a putative mechanism in addiction liability. *Int J Neuropsychopharmacol*. 2014. <https://doi.org/10.1093/ijnp/pyu001>.
36. Weksler B, Romero IA, Couraud P-O. The hCMEC/D3 cell line as a model of the human blood brain barrier. *Fluids Barriers CNS*. 2013;10(1):16.
37. Saaby L, Helms HC, Brodin B. IPEC-J2 MDR1, a novel high-resistance cell line with functional expression of human P-glycoprotein (ABCB1) for Drug Screening Studies. *Mol Pharm*. 2016;13(2):640–52.
38. Boron WF, De Weer P. Intracellular pH transients in squid giant axons caused by CO₂, NH₃, and metabolic inhibitors. *J Gen Physiol*. 1976;67(1):91–112.
39. Eneberg E, Jones CR, Jensen T, Langthaler K, Bundgaard C. Practical application of rodent transporter knockout models to assess brain penetration in drug discovery. *Drug Metab Bioanal Lett*. 2022;15(1):12–21.
40. Langthaler K, Jones CR, Brodin B, Bundgaard C. Assessing extent of brain penetration in vivo (Kp, uu, brain) in Göttingen minipig using a diverse set of reference drugs. *Eur J Pharm Sci*. 2023;190:106554.
41. Rubio-Beltrán E, Labastida-Ramírez A, Villalón CM, MaassenVanDenBrink A. Is selective 5-HT_{1F} receptor agonism an entity apart from that of the triptans in antimigraine therapy? *Pharmacol Ther*. 2018;186:88–97.
42. DrugBank online. Almotriptan DB00918; Eletriptan DB00216, Frovatriptan DB00998, Naratriptan DB00952, Rizatriptan DB00953, Sumatriptan DB00669, Zolmitriptan DB00315, Oxycodone DB00497, Pyrilamine DB06691. <https://go.drugbank.com/drugs>. Accessed 23 Feb 2023.
43. PubChem. PubChem Compound Summary for: Almotriptan; Eletriptan; Frovatriptan; Naratriptan; Sumatriptan; Zolmitriptan; Oxycodone; Pyrilamine. <https://pubchem.ncbi.nlm.nih.gov>. Accessed 23 Feb 2023.
44. ChemSpider. Almotriptan; Eletriptan; Frovatriptan; Naratriptan; Rizatriptan; Sumatriptan; Zolmitriptan; Oxycodone; Pyrilamine. <https://www.chemspider.com/>. Accessed 23 Feb 2023.
45. Leslie EM, Deeley RG, Cole SP. Multidrug resistance proteins: role of P-glycoprotein, MRP1, MRP2, and BCRP (ABCG2) in tissue defense. *Toxicol Appl Pharmacol*. 2005;204(3):216–37.
46. Sharom FJ. ABC multidrug transporters: structure, function and role in chemoresistance. *Pharmacogenomics*. 2008;9(1):105–27.
47. Ozgur B, Saaby L, Langthaler K, Brodin B. Characterization of the IPEC-J2 MDR1 (iP-gp) cell line as a tool for identification of P-gp substrates. *Eur J Pharm Sci*. 2018;112:112–21.

48. Loryan I, Sinha V, Mackie C, Van Peer A, Drinkenburg W, Vermeulen A, et al. Mechanistic understanding of brain drug disposition to optimize the selection of potential neurotherapeutics in drug discovery. *Pharm Res.* 2014;31(8):2203–19.
49. Doetsch DA, Ansari S, Jensen O, Gebauer L, Dücker C, Brockmüller J, et al. Substrates of the human brain proton-organic cation antiporter and comparison with organic cation transporter 1 activities. *Int J Mol Sci.* 2022. <https://doi.org/10.3390/ijms23158430>.
50. Cheng Z, Liu H, Yu N, Wang F, An G, Xu Y, et al. Hydrophilic anti-migraine triptans are substrates for OATP1A2, a transporter expressed at human blood-brain barrier. *Xenobiotica.* 2012;42(9):880–90.
51. Wilt LA, Nguyen D, Roberts AG. Insights into the molecular mechanism of triptan transport by P-glycoprotein. *J Pharm Sci.* 2017;106(6):1670–9.
52. Evans DC, O'Connor D, Lake BG, Evers R, Allen C, Hargreaves R. eletriptan metabolism by human hepatic cyp450 enzymes and transport by human P-glycoprotein. *Drug Metab Dispos.* 2003;31(7):861–9.
53. Mahar Doan KM, Humphreys JE, Webster LO, Wring SA, Shampine LJ, Serabjit-Singh CJ, et al. Passive permeability and P-glycoprotein-mediated efflux differentiate central nervous system (CNS) and non-CNS marketed drugs. *J Pharmacol Exp Ther.* 2002;303(3):1029–37.
54. Tfelt-Hansen P, Edvinsson L. Pharmacokinetic and pharmacodynamic variability as possible causes for different drug responses in migraine. *Comment Cephalalgia.* 2007;27(10):1091–3.

Publisher's Note

Springer Nature remains neutral with regard to jurisdictional claims in published maps and institutional affiliations.